NRC Research Press

ARTICLE

Induced energy polarization of the vacuum and the rotational curve for the Galaxy

A. Raymond Penner

Abstract: The theory of an induced energy polarized vacuum, as previously presented by the author (Penner. *Can. J. Phys.* **90**, 315 (2012)), is used to generate a theoretical rotational curve for the Galaxy. The theoretical curve generated is found to be in good agreement with Sofue's (*Publ. Astron. Soc. Jpn.* **64**, (In press) (2012)) compilation of observations. For the baryonic mass distribution and baryonic Tully–Fisher relationship that is used, the theoretical orbital velocity at the Sun's location is found to be (235 ± 15) km s^{-1}. The galactic rotational velocity is then found to slowly fall from this value as it asymptotically approaches the value of (192 ± 15) km s^{-1}.

PACS No.: 90.95.30.–k.

Résumé : Nous utilisons la théorie du vide polarisé à énergie induite développée par l'auteur (Penner. *Can. J. Phys.* **90**, 315 (2012)), afin de générer une courbe théorique de vitesse de rotation pour la galaxie. La courbe théorique ainsi générée est en bon accord avec les observations compilées par Sofue (*Publ. Astron. Soc. Jpn.* **64**, (In press) (2012)). Pour la distribution de masse baryonique et la relation baryonique de Tully–Fisher utilisées, nous trouvons qu'à la localisation du Soleil, la vitesse orbitale théorique est de (235 ± 15) km s^{-1}. La vitesse galactique tombe alors lentement pour approcher la valeur asymptotique de (192 ± 15) km s^{-1}. [Traduit par la Rédaction]

1. Introduction

Rotational curves are a primary tool used in determining the mass distribution of galaxies. Indeed, the fact that the determined mass distributions do not match the stellar distributions is a major reason for the dark matter hypothesis. Examples of galactic rotational curves are provided by Sofue [1], Sofue et al. [2], and Noodermeer et al. [3]. There are two general characteristics that are found with these galactic rotational curves. First, the stellar orbital velocities do not fall off with increasing distance, as expected. Instead, as one moves further from the galactic center, the rotational velocity curves typically flatten out and the rotational velocity remains relatively constant. Second, there is a relationship between this constant orbital velocity found at large distances and the total luminosity of galaxies. This is called the Tully–Fisher [4] relationship. By taking into account the gas content of galaxies, it has been shown by McGaugh et al. [5] that this relationship is fundamentally a relationship between *v*, the rotational velocity of galaxies; and *M*, their total baryonic mass. This baryonic Tully–Fisher relationship (BTFR) as given by McGaugh and Wolf [6] is

$$M = AM_{\odot}v^4 \tag{1}$$

with $A = (45 \pm 10)$ km^{-4} s^4.

The current theory of dark matter can handle the flattening out of galactic rotation curves by having the dark matter cluster with a density that varies with distance from the galactic nucleus as r^{-2}. However, such a distribution does not fall out naturally from the theory. The BTFR is even more difficult to explain, as it implies a strong correlation between baryonic matter and dark matter.

The flattening out of galactic rotation curves and the BTFR are motivating factors behind alternatives to the dark matter theory. As a prime example, modified Newtonian dynamics (MOND), as proposed by Milgrom [7–9], postulates that the inertia of an object varies with acceleration in such a manner so as to specifically produce the BTFR. A review of MOND and other alternatives to the dark matter theory is provided by Mannheim [10].

In Penner [11, 12], the author proposed a new alternative to dark matter, again inspired by the flattening out of galactic rotation curves and the BTFR. In this theory, baryonic matter induces a gravitational contribution from the vacuum. An overview of this theory will be provided in Sect. 2.

The focus of this particular paper will be on applying the author's theory as given in Penner [12] to the rotational curve of the Galaxy. Unlike dark matter models, in the author's theory there are no free parameters to adjust to provide the best fit to a given rotational curve. The contribution of the vacuum to the gravitational field is determined directly by the baryonic mass distribution and the coefficient of the BTFR. The resulting theoretical rotational curve will then be compared with the grand rotational curve for the Galaxy as provided by Sofue [13–15], who compiled kinematical data from the literature. Sofue scaled the different observations to a solar rotational velocity of 200 km s^{-1} and determined a running mean of the compiled data (Sofue [13]) leading to the result shown in Fig. 1. Included are the circular velocities from Sloan Digital Sky Survey blue star analyses by Xue et al. [16], and rotational velocities from VERA for stellar maser sources (Honma et al. [17], Oh et al. [18]). The scale value of 200 km s^{-1} used by Sofue for the solar rotational velocity is below the recommended IAU value of 220 km s^{-1}. Indeed, it is far below the value of (254 ± 16) km s^{-1} obtained by Reid et al. [19]. Their value was obtained using the Very Long Baseline Array and the Japanese Very Long Baseline Interferometry Exploration of Radio Astronomy project to mea-
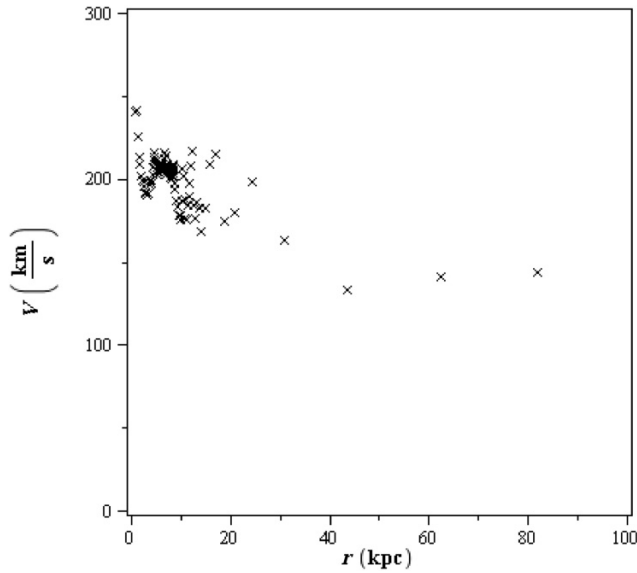
Can. J. Phys. **91**: 1–8 (2013) dx.doi.org/10.1139/cjp-2012-0300

Published at www.nrcresearchpress.com/cjp on 21 November 2012.

Fig. 1. A running mean of the data compiled by Sofue [13].

sure trigonometric parallaxes and proper motion of masers found in star-forming regions across the Galaxy.

The outline of this paper is as follows. In Sect. 2, an overview of the theory in Penner [12] will be presented. In Sect. 3, a theoretical rotational curve of the Galaxy will be generated using a model of the baryonic mass distribution of the Galaxy and the author's theory. This theoretical rotational curve will then be compared with the observed values as summarized in Fig. 1. In addition, the effect that possible variations in the theory would have on the theoretical rotational curve will be considered. This will be followed by a conclusion and a discussion on issues related to the theory of an induced energy polarized vacuum.

2. Theory

2.1. General consequences of an induced energy polarized vacuum

Without reference to the specific nature of the entities, consider the consequences of the vacuum consisting of entities that in some manner become polarized with respect to energy in the presence of a gravitational field. The induced energy dipole moment density, $\boldsymbol{P}_E$, would be given by

$$\boldsymbol{P}_E = n\boldsymbol{p}_E \qquad (2)$$

where n is equal to the number of entities per unit volume and $\boldsymbol{p}_E$ is the induced energy dipole moment per entity. The resulting energy density of the vacuum, ρ_E, surrounding a given gravitational field source is then given by

$$\rho_E = -\nabla \cdot \boldsymbol{P}_E \qquad (3)$$

and by Gauss's law for gravitation the total gravitational field, $\boldsymbol{g}$, will be determined from

$$\nabla \cdot \boldsymbol{g} = -\frac{4\pi G}{c^2}(\rho_M + \rho_E) \qquad (4)$$

where ρ_M is the energy density of the baryonic mass.

The resulting gravitational field contribution, $\boldsymbol{g}_A$, because of this energy polarized vacuum will be given by

$$\boldsymbol{g}_A = \frac{G}{c^2} \int_{V'} \frac{\rho_E dV'}{(r-r')^3}(\boldsymbol{r}-\boldsymbol{r}') \qquad (5)$$

In the case of spherical symmetry or in the far field limit where $r \to \infty$, (5), with the use of (3), simplifies to

$$\boldsymbol{g}_A = \frac{4\pi G}{c^2}\boldsymbol{P}_E \qquad (6)$$

Consider first the case where the dependence of the induced energy dipole moment density on the total gravitational field, $\boldsymbol{g}$, is linear such that

$$\boldsymbol{P}_E = \kappa\frac{c^2}{4\pi G}\boldsymbol{g} \qquad (7)$$

where κ is a dimensionless constant. Then by (3), (4), and (7)

$$\rho_E = \frac{\kappa}{1-\kappa}\rho_M \qquad (8)$$

and the resulting relationship between the total gravitational field and g_M, the gravitational field due to the baryonic mass, will be given by

$$\boldsymbol{g} = \frac{1}{1-\kappa}\boldsymbol{g}_M \qquad (9)$$

The consequences of a linearly induced energy polarized vacuum will therefore be that the apparent mass of the baryonic source will increase by a factor of $1/(1-\kappa)$ but the surrounding gravitational field will still fall off as the inverse square of the distance. The effects of an induced energy polarized vacuum in this case would not be apparent.

Consider now the case where the relationship between the induced energy dipole moment density and the gravitational field is nonlinear. In the far field limit, where $g \ll g_0$ with g_0 being a constant to be determined, this nonlinear relationship can, in general, be expanded as

$$\boldsymbol{P}_E = \kappa\frac{c^2}{4\pi G}g_0\left\{\left(\frac{g}{g_0}\right) - \beta\left(\frac{g}{g_0}\right)^2 + \mathbb{O}\left[\left(\frac{g}{g_0}\right)^3\right]\right\}\hat{\boldsymbol{g}} \qquad (10)$$

where κ and β are dimensionless constants. In the far field, where the gravitational field from the induced energy polarized vacuum dominates, (i.e., for $g/g_0 \ll 1$, $g_A \to g$), by (6) and (10) it follows that $\kappa = 1$. The far field gravitational field contribution of the induced energy polarized vacuum will therefore be given by

$$g_A = g_0\left\{\left(\frac{g}{g_0}\right) - \beta\left(\frac{g}{g_0}\right)^2 + \mathbb{O}\left[\left(\frac{g}{g_0}\right)^3\right]\right\} \qquad (11)$$

Substituting $g = g_M + g_A$ into (11) and keeping only terms up to second order leads to the following far field relationship between the total gravitational field and the gravitational field due to the baryonic mass:

$$g^2 = \frac{g_M g_0}{\beta} \qquad (12)$$

The far field gravitational field in the case of a nonlinearly induced energy polarized vacuum will therefore in general fall off as $g_M^{1/2}$ or as $1/r$. Such an effect would be very apparent. By the substitutions $g = v^2/r$ and $g_M = GM/r^2$, (12) can also be expressed as the following relationship between the total baryonic mass and the far field orbital velocity:

$$M = \frac{\beta}{Gg_0}v^4 \tag{13}$$

The baryonic Tully–Fisher relationship between the baryonic mass of a galaxy and the galaxy's rotational velocity is therefore a natural consequence of the relationship between the induced energy polarization of the vacuum and the gravitational field being nonlinear. The details of the nonlinearity will determine the values of β and g_0 in (13) but not this general result. Equating the coefficients of (13) and (1) results in

$$\frac{g_0}{\beta} = (1.7 \pm 0.4) \times 10^{-10} \text{ m s}^{-2} \tag{14}$$

2.2. Model of the energy polarization of the vacuum

In Penner [12] a semiclassical model of how the vacuum becomes energy polarized in the presence of a gravitational field is provided. A summary of this model is as follows where some of the equations from Penner [12] have been reworked to maintain consistency with Sect. 2.1.

It is hypothesized in Penner [12] that throughout the cosmos entities of both net positive energy and net negative energy continually come into and out of existence with a maximum lifetime, τ, as given by the Heisenberg uncertainty principle;

$$\tau \cong \frac{\bar{h}}{2|E|} \tag{15}$$

where E is the net energy of a given entity. During a given entity's lifetime it will be attracted to a gravitational source if its energy is positive and repelled from the source if its energy is negative. Each entity will therefore have an equivalent energy dipole moment, p_E, given by

$$p_E = E\langle x \rangle_t \tag{16}$$

where $\langle x \rangle_t$ is the time-averaged displacement of the entity that is due to the gravitational field. For both positive and negative energy entities p_E will point in the direction of the gravitational field. In Penner [12] the entities are modeled as coming into existence with zero velocity with respect to the gravitational field and as such

$$\langle x \rangle_t = \frac{1}{3}x_A \tag{17}$$

where

$$x_A = \frac{1}{2}gt_E^2 \tag{18}$$

with $t_E \leq \tau$ being the lifetime of a given entity.

The equivalent energy dipole moment density will be given by

$$P_E = N \overline{p_E t_E} \tag{19}$$

where N is the rate per unit volume at which entities (both positive and negative) come into existence, and the bar over $p_E t_E$ represents an averaging over the entities. By (16)–(19) it then follows that

$$P_E = \frac{1}{3}\sqrt{\frac{2}{g}} NE \overline{x_A^{3/2}}\hat{g} \tag{20}$$

If the entities do not interact with each other their lifetime, t_E, is taken to be equal to τ and by (18) and (20)

$$P_E = \left(\frac{1}{6}NE\tau^3\right)g \tag{21}$$

and the relationship between the energy dipole moment density and the gravitational field is linear. As discussed in Sect. 2.1, for a linear relationship the effect of an induced energy polarized vacuum will not be apparent.

However, in the model presented by Penner [12] interactions between the entities are explicitly considered. In the model if a positive energy entity interacts with a negative energy entity both entities cease to exist. In this case

$$\overline{x_A^{3/2}} = \int_0^\alpha x_A^{3/2} P(x)\mathrm{d}x + \alpha^{3/2}\int_\alpha^\infty P(x)\mathrm{d}x \tag{22}$$

where $P(x)$ is the probability function for the distance travelled by an entity before interacting with another entity and

$$\alpha = \frac{1}{2}g\tau^2 \tag{23}$$

is the maximum distance an entity can travel. The probability function will be given by the standard Beer–Lambert law;

$$P(x) = \mu e^{-\mu x} \tag{24}$$

where μ, the attenuation coefficient, is given by

$$\mu = \sigma n_i \tag{25}$$

with σ being the cross-sectional area for an interaction and n_i is the number density of the entities that can take part in an interaction. Evaluating (22) then leads to

$$\overline{x_A^{3/2}} = \frac{\sqrt{\alpha}}{\mu}\frac{3}{2}(\gamma - e^{-\alpha\mu}) \tag{26}$$

where

$$\gamma = \frac{\sqrt{\pi}}{2}\frac{\mathrm{erf}\left(\sqrt{\alpha\mu}\right)}{\sqrt{\alpha\mu}} \tag{27}$$

In Penner [12] it is shown that the attenuation coefficient can be expressed as

$$\mu = \gamma\mu_0 \tag{28}$$

where

$$\mu_0 = \frac{1}{2}N\sigma\tau \qquad (29)$$

is the attenuation coefficient in the far field limit. From (20) and (22)–(29) the induced energy density dipole moment is then given by

$$P_E = \frac{NE\tau}{3\mu_0}\left[\frac{3}{2}\left(1 - \frac{e^{-\gamma(g/g_0)}}{\gamma}\right)\right]\hat{g} \qquad (30)$$

where

$$g_0 = \frac{2}{\mu_0\tau^2} \qquad (31)$$

In the far field limit, where $g/g_0 \ll 1$, the expression in the brackets of (30) approaches g/g_0. In addition, in the case where in the far field the gravitational field from the induced energy polarized vacuum dominates, (i.e., for $g/g_0 \ll 1$, $g_A \rightarrow g$), by (6) and (30) it then follows that

$$\frac{NE\tau}{3\mu_0} = \frac{c^2}{4\pi G}g_0 \qquad (32)$$

Therefore by (30) and (32) the dependence of the induced energy dipole moment density on the gravitational field can be expressed as

$$P_E = \frac{c^2}{4\pi G}g_0\left[\frac{3}{2}\left(1 - \frac{e^{-\gamma(g/g_0)}}{\gamma}\right)\right]\hat{g} \qquad (33)$$

where by (23), (31), and (27)–(29)

$$\gamma = \frac{\sqrt{\pi}}{2}\frac{\text{erf}\left[\sqrt{\gamma(g/g_0)}\right]}{\sqrt{\gamma(g/g_0)}} \qquad (34)$$

In the far field limit it is shown in Penner [12] that the expression in the brackets of (33) can be expanded as

$$\frac{3}{2}\left(1 - \frac{e^{-\gamma(g/g_0)}}{\gamma}\right) = \left(\frac{g}{g_0}\right) - \frac{3}{5}\left(\frac{g}{g_0}\right)^2 + \mathbb{O}\left[\left(\frac{g}{g_0}\right)^3\right] \qquad (35)$$

Therefore by (6), (33), and (35) the far field gravitational field due to the energy polarized vacuum is

$$g_A = g_0\left\{\left(\frac{g}{g_0}\right) - \frac{3}{5}\left(\frac{g}{g_0}\right)^2 + \mathbb{O}\left[\left(\frac{g}{g_0}\right)^3\right]\right\} \qquad (36)$$

Comparing (36) with (11) it can be seen that the value of β for this model is 3/5 resulting in a value for g_0, from (14), of[1]

$$g_0 = (1.0 \pm 0.2) \times 10^{-10} \text{ m s}^{-2} \qquad (37)$$

Figure 2 shows the energy dipole moment density P_E, as per (33), as a function of the gravitational field g. As is seen in the figure for

Fig. 2. The theoretical relationship between the induced energy dipole moment density, P_E, and the gravitational field, g.
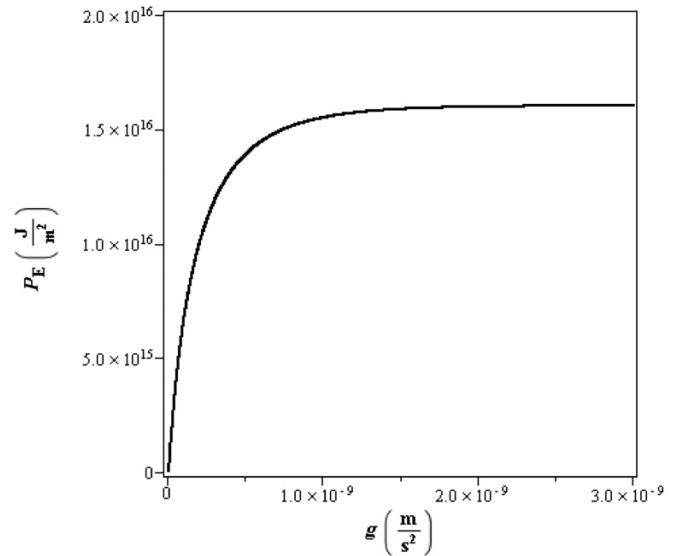
a value of $g_0 = 1.0 \times 10^{-10}$ m s^{-2} the value of p_E approaches a constant value of 1.6×10^{16} J m^{-2}. Although variations of the modeled entities behaviour are possible the saturation indicated by Fig. 2 would be a common feature. For spherical symmetry the value of g_A will, by (6), also approach a constant value as the gravitational field increases. The strong field value in this case is[1]

$$g_A \rightarrow (1.5 \pm 0.4) \times 10^{-10} \text{ m s}^{-2} \qquad (38)$$

3. Rotational curve of the Galaxy

3.1. Baryonic mass distribution and resulting gravitational field

Flynn et al. [20] provide estimates of the stellar mass of the Galaxy based on measurements of the volume luminosity density and surface luminosity density generated by the local galactic disk. The stellar mass determined is a function of the assumed exponential disk scalelength, R_D. The resulting stellar mass of the Galaxy is 48.5−55 × 10^9 M$_\odot$ for 2 kpc ≤ R_D ≤ 5.5 kpc. The total gas mass is estimated at $(9.5 \pm 3) \times 10^9$ M$_\odot$ yielding a total baryonic mass for the Galaxy of $(61 \pm 5) \times 10^9$ M$_\odot$. The breakdown of the contribution from the disc and the bulge is also dependent on the scalelength. For an R_D of 3 kpc the ratio of the stellar mass in the disc to that of the bulge is found to equal 1.92. Using as an approximation that the distribution of the gas follows that of the stellar mass and using a value for R_D = 3 kpc then leads to the following baryonic mass distribution of the Galaxy:

$$M_{TOTAL} = (61 \pm 5) \times 10^9 \text{ M}_\odot \qquad (39a)$$

$$M_{DISC} = (40 \pm 3) \times 10^9 \text{ M}_\odot \qquad (39b)$$

$$M_{BULGE} = (21 \pm 2) \times 10^9 \text{ M}_\odot \qquad (39c)$$

The gravitational potential in cylindrical coordinates for an exponential disc can be shown to be given by

---

[1]In Penner [12] an older estimate for A of 35 km^{-4} s^4 (McGaugh et al. [5]) was used in equation (1) thereby leading to slightly different values.

$$\Phi_{\text{DISC}}(r, z) = -\frac{2G}{\pi}\frac{M_{\text{DISC}}}{R_D^2}\int_0^\infty \frac{xe^{-x/R_D}K\left(\sqrt{4xr/q^2}\right)}{q}dx \qquad (40a)$$

where

$$q = \sqrt{z^2 + (x + r)^2} \qquad (40b)$$

and K is the complete elliptic integral of the first kind. For the bulge component the following Hernquist model was used with the scalelength $R_B = 0.4$ kpc:

$$\Phi_{\text{BULGE}}(r) = -\frac{GM_{\text{BULGE}}}{r + R_B} \qquad (41)$$

The resulting baryonic gravitational fields are then determined from

$$\mathbf{g}_{\text{DISC}} = -\nabla\Phi_{\text{DISC}} \qquad (42)$$

and

$$\mathbf{g}_{\text{BULGE}} = -\nabla\Phi_{\text{BULGE}} \qquad (43)$$

3.2. Theoretical rotational curve

Given the relationship between the induced energy dipole moment density, P_E, and the gravitational field, $\mathbf{g}$, as given by (33) along with (3) and (5) the total gravitational field surrounding the Galaxy can be determined. One complication is that (5) is a transcendental equation as ρ_E, through P_E in (3), is a function of $\mathbf{g}$, which in turn is a function of $\mathbf{g}_A$. The method of solution is as follows. The initial estimate of the gravitational potential and the gravitational field surrounding the Galaxy is taken to be solely that due to the baryonic mass. The value of P_E and the resulting energy density of the vacuum are then determined by (33) and (3). From the energy density distribution the gravitational potential due to the vacuum is then determined and for the next estimate the total gravitational potential is taken to be equal to the sum of the potentials due to the baryonic mass and the vacuum. This iterative process is then repeated until the resulting values of the gravitational field obtained after a given iteration vary by less than 1% from the previous iteration.

From the resulting total gravitational field, $\mathbf{g}$, as well as from $\mathbf{g}_{\text{DISC}}$, $\mathbf{g}_{\text{BULGE}}$, and $g_A = (g^2 - g_{\text{DISC}}^2 - g_{\text{BULGE}}^2)^{1/2}$, the corresponding contributions to the rotational velocity were determined, i.e., $v = (rg)^{1/2}$. The result for $g_0 = 1.0 \times 10^{-10}$ m s^{-2} and a baryonic mass of 61×10^9 M$_\odot$ is shown in Fig. 3. The baryonic Tully–Fisher rotational velocity, as determined from (1) and (39a), is (192 ± 15) km s^{-1}. As is seen in Fig. 3, this is the value that the rotational curve due to the vacuum contribution asymptotically approaches. The overall rotational curve initially follows that of the bulge, has a slight dip at 3 kpc followed by a broad maximum between 5 and 10 kpc, which encompasses the position of the Sun. The details of these features will be dependent on the scalelengths chosen for the disc and bulge as well as their assigned baryonic masses. The theoretical rotational velocity found at the location of the Sun ($r = 8$ kpc) is (235 ± 15) km s^{-1}, which is well within the range given by Reid et al. [19]. The rotational velocity then slowly drops as it asymptotically approaches the value of (192 ± 15) km s^{-1}. The theoretical rotational velocity will then remain at this value until other galaxies start having a significant influence on the overall gravitational field.

Fig. 3. The contribution of the bulge (o), the disc (◇) and the polarized vacuum (□) to the net rotational curve (·) of the galaxy.
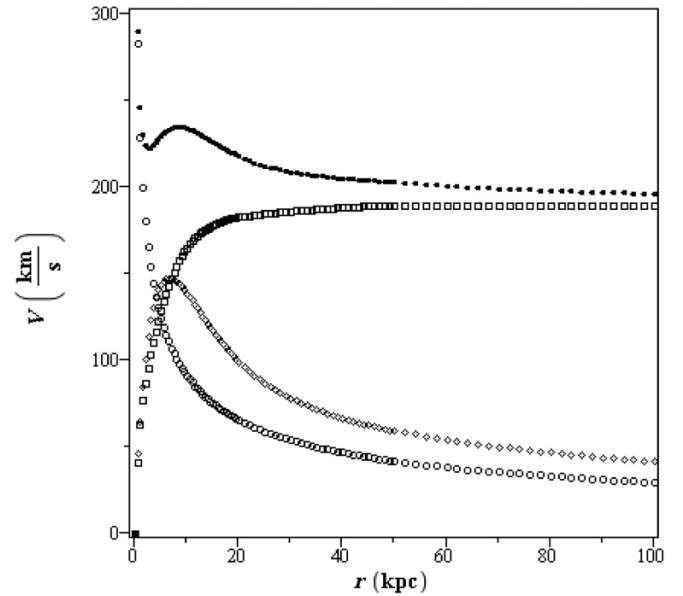
The theoretical curve generated has systematically higher velocity values than the experimental curve provided by Sofue (i.e., Figure 1). However, as stated in the introduction, Sofue scaled the observations so that the rotational velocity of the Sun is 200 km s^{-1}. To better compare the theoretical rotational curve with the compilation of results provided by Sofue [13], Sofue's values will therefore be scaled up by 35 km s^{-1} so that both the experimental and theoretical solar rotational velocities are equal to 235 km s^{-1}. The result is shown on Fig. 4. Overall for $r < 20$ kpc the agreement is quite good. The theoretical baryonic mass distribution that was used ignored features, such as the spiral arms, so the details within 10 kpc should not be taken as significant. Beyond 20 kpc the agreement is still good, especially considering the large uncertainties in Sofue's values. Sofue also provided values beyond 100 kpc, however, at those distances the effects of the neighbouring galaxies would be significant.

3.3. Dependence on variations in the model

The model of how the vacuum becomes energy polarized in the presence of a gravitational field presented by the author [12] and in Sect. 2.2 involves several simplifications. To determine how sensitive the generated rotation curve is to possible variations in the model, rotation curves were generated for two other induced energy dipole moment density functions. These functions are as follows:
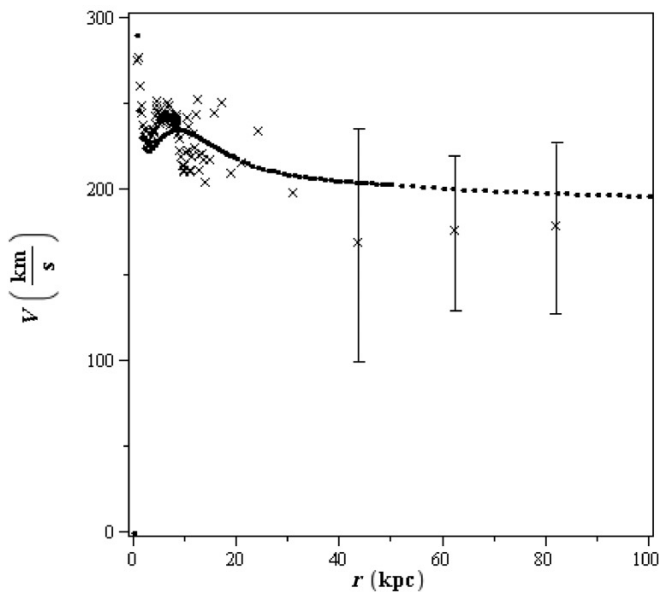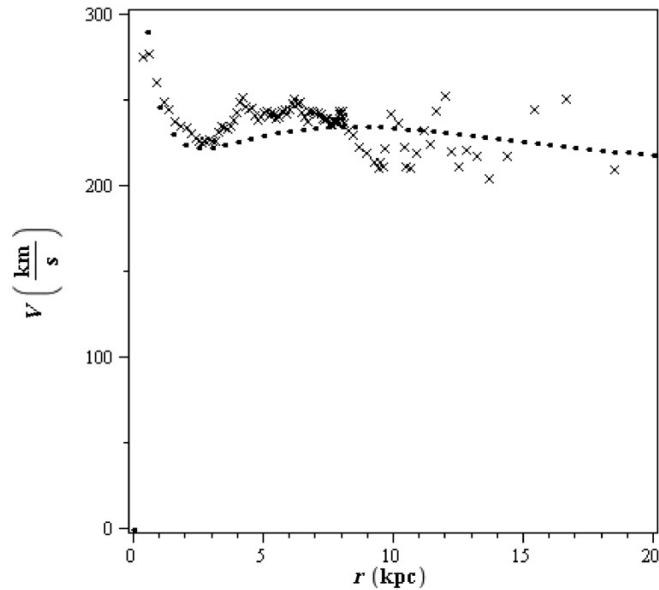
$$P_E = \frac{c^2}{4\pi G}g_0^*\left[1 - e^{-(g/g_0^*)}\right] \qquad (44)$$

and

$$P_E = \frac{c^2}{4\pi G}g_0^*\ln\left(1 + \frac{g}{g_0^*}\right) \qquad (45)$$

For $g/g^* \ll 1$, both these functions can be expanded as a series, and for both, $\beta = 1/2$, resulting in g_0^* from (14), being equal to 0.84×10^{-10} m s^{-2}. These two functions are plotted in Fig. 5 along with the theoretical induced energy dipole moment density function as

Fig. 4. The theoretical rotational curve (·) compared with Sofue's compiled data (x). Uncertainties in Sofue's results are shown for $r > 40$ kpc.

Fig. 5. The induced energy dipole moment density as given by (44) (lower curve), (45) (upper curve) and the theoretical relationship as given by (33) (middle curve).

Fig. 6. The generated rotational curves as derived using the induced energy dipole moment density as given by (44) (lower curve), (45) (upper curve) and the theoretical relationship as given by (33) (middle curve).
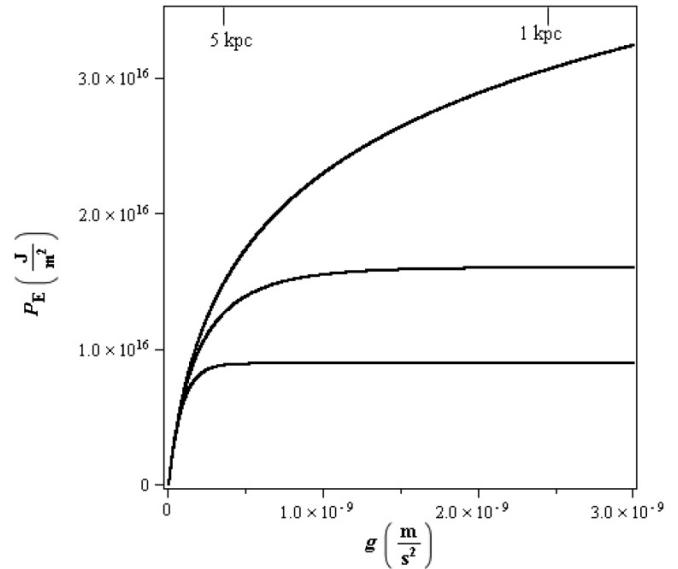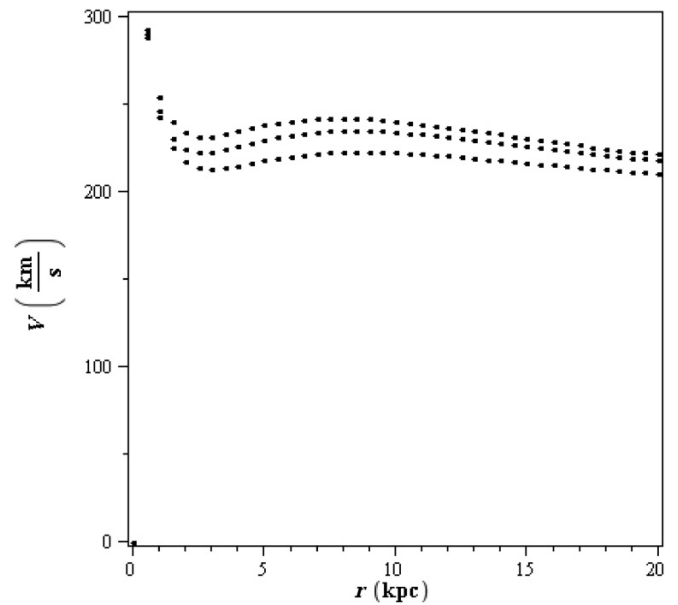

given by (33). The theoretical rotational curves generated by all three functions are shown in Fig. 6. As seen in Fig. 5, although the functions of P_E as given by (44) and (45) vary significantly from the theoretical function, the effects on the rotational curves as seen in Fig. 6 are only secondary. The reason being that the differences between the functions are greatest where the gravitational field is the strongest. As indicated on Fig. 5 this corresponds to $r \lesssim 5$ kpc. This, however, corresponds to the region where the relative contribution to the gravitational field provided by the induced energy polarized vacuum is less than that provided by the baryonic mass. Hence variations in the modeled behavior of the entities will have limited impact on generated rotational curves. The solar velocity found for the functions given by (44) and (45) are 223 and 242 km s^{-1}, respectively. If the rotational velocity of the Sun could be determined more precisely it would then be possible to distinguish between different possible models for the induced energy polarization of the vacuum.

4. Conclusion

The theory of an induced energy polarized vacuum as previously presented by the author [12] has been used to generate a rotational curve for the Galaxy. This is found to be in good agreement with Sofue's compilation of results. For the given baryonic mass distribution model and BTFR coefficient the theoretical orbital velocity at the Sun's location was found to be (235 ± 15) km s^{-1}. The Galactic rotational velocity is then found to slowly fall from this value as it asymptotically approaches the value of (192 ± 15) km s^{-1}.

The Milky Way Galaxy's rotational curve was chosen as the first application of the author's theory of an induced energy polarized vacuum for the primary reason that it is our galaxy. Future work will consider in more general terms the nature of galactic rotational curves that are generated by the theory.

5. Discussion

For the given model of the induced energy polarized vacuum some of the details of the entities can be determined. Expressing the interaction cross section, σ, as equal to πr_0^2, where r_0 is the range of the interaction, the following inequality would be expected to hold:

$$N\tau < \left(\frac{4}{3}\pi r_0^3\right)^{-1} \tag{46}$$

where $N\tau$ is the maximum entity density (i.e., the number density of entities in the far field or zero gravitational field limit). Equation (46) basically states that the average separation of the entities is greater than their interaction range. Equations (46), (15), (29), (31), and (32) along with the value of g_0 as given by (37) then lead to the following inequalities[1]:

$$r_0 < 2.9 \times 10^{-23}\ \text{m} \tag{47a}$$

$$\sigma < 2.6 \times 10^{-45}\ \text{m}^2 \tag{47b}$$

$$|E| < 4.2 \times 10^{-29}\ \text{J} \quad \text{and} \tag{47c}$$

$$\tau > 1.2 \times 10^{-6}\ \text{s} \tag{47d}$$

From (47b) and (47c) it is seen that the entities would appear to be weakly interacting particles of very small energy.

To facilitate an understanding of the theory of an energy polarized vacuum a numerical example where the interaction range, r_0, is equal to 1×10^{-23} m, in agreement with (47a), will be considered. Given this value of r_0 it follows from (15), (29), (31), (32), and (37) that

$$\sigma = 3.1 \times 10^{-46}\ \text{m}^2 \tag{48a}$$

$$|E| = 5.1 \times 10^{-30}\ \text{J} \tag{48b}$$

$$\tau = 1.0 \times 10^{-4}\ \text{s} \quad \text{and} \tag{48c}$$

$$N = 1.1 \times 10^{71}\ \text{m}^{-3}\text{s}^{-1} \tag{48d}$$

The resulting energy densities of the positive and negative energy entities in the zero gravitational or far field limit for this example are then given by

$$\rho_+ = |\rho_-| = \frac{1}{2}NE\tau \tag{49a}$$

$$\rho_+ = 3.0 \times 10^{28}\ \text{J}\ \text{m}^{-3} \tag{49b}$$

The magnitudes of the energy densities for the positive and negative entities are certainly very large. Of course in the absence of a gravitational field the two energy densities will cancel each other and the net energy density, ρ_E, of the vacuum will equal zero. In a gravitational field this is no longer the case as the entities will shift and interact as per the model outlined in Sect. 2.2; ρ_+ will no longer be equal in magnitude to ρ_- and the net energy density of the vacuum, $\rho_E = \rho_+ + \rho_-$, will no longer equal zero but will equal the value given by (3). For example, at the

position of the Sun, ($r = 8$ kpc), ρ_E is determined by the model to be equal to 2.2×10^{-4} J m^{-3}. Comparing this value to (49b) it is seen that the relative change in the energy densities of the entities in the presence of a gravitational field is extremely small. However, the resulting contribution that ρ_E makes to the gravitational field of a galaxy is very large and is responsible for the observed galactic rotational curves as well as the BTFR. Although the value of r_0 used and the resulting values given by (48a)–(48d) is just to be taken as an example, the general conclusions would be expected to hold.

With regards to the author's induced energy polarized vacuum theory there are several issues that have been raised by reviewers. First, as the theory leads naturally to the BTFR, the exponent in the relationship between the baryonic mass and the asymptotic rotation velocity, as given by (1), has to be exactly 4. The BTFR is found to be in good agreement with observations of galaxies with masses ranging over approximately seven orders of magnitude (i.e., from approximately 10^{12} M$_\odot$ down to 10^5 M$_\odot$). However, significant deviations from the BTFR have been observed with the faintest Local Group dwarf galaxies, which have masses $<10^5$ M$_\odot$. McGaugh and Wolf [6] present several possible explanations for these deviations. Of particular interest is the correlation between the extent of the deviation from the BTFR and the dwarfs' susceptibility to tidal influences from their host galaxy. In the theory of an induced energy polarized vacuum there would be expected to be an even greater effect. Those dwarfs that are the most susceptible to tidal effects will also be those dwarfs that have their surrounding vacuum energy density distribution most distorted by the host galaxy. Dwarf galaxies orbiting a host galaxy cannot be treated as isolated systems in the author's theory and the BTFR would not be expected to apply to them.

A second issue relates to the saturation value as given by (38). Within the solar system the gravitational field due to the Sun is many orders of magnitude greater than the fields involved in the generation of the Galaxy's rotation curve. As such, if the author's model is extended to the solar system, the value of g_A is found to be at the saturated value of $(1.5 \pm 0.4) \times 10^{-10}$ m s^{-2}. This is tantalizingly close to the value of the Pioneer anomaly [21–23], which is given by

$$a_{\text{PIONEER}} = (8.74 \pm 1.33) \times 10^{-10}\ \text{m}\ \text{s}^{-2} \tag{50}$$

In Penner [12], the author attempted to explain the difference between the lower theoretical value and the higher observed value, as given by (50), by postulating that the positive and negative energy entities have more than one energy magnitude. An example is presented in Penner [12] where entities of two different energy levels can lead to the higher value. However, given the recent results of Turyshev et al. [24] the necessity to explain the lower theoretical value no longer exists. By modeling the emission of thermal radiation off of the Pioneer vehicles, Turyshev et al. found that the bulk of the anomalous acceleration can be explained. Using their Fig. 3, the anomalous acceleration over the distance of 20 to 70 AU is estimated at $(1.4 \pm 1.9) \times 10^{-10}$ m s^{-2}, with the given uncertainty being solely due to the modeling of the thermal term. Turyshev et al. conclude "that at the present level of our knowledge of the Pioneer 10 spacecraft and its trajectory, no statistically significant acceleration anomaly exists." Although the simplest possibility is that the anomalous acceleration is zero, the value of $(1.5 \pm 0.4) \times 10^{-10}$ m s^{-2} derived from the induced energy polarized vacuum theory is actually in very good agreement with these results. The uncertainties are just too large to draw any conclusions.

An issue with Turyshev et al.'s result is that their thermal induced acceleration value increased when the spacecraft was closer to the Sun early in its trajectory. The anomalous Pioneer acceleration has a very distinct onset between 10 and 20 AU, and

while the spacecraft was in the inner solar system no anomalous acceleration was measured. Turyshev et al. suggest that this discrepancy, within the inner solar system, between their results and the Pioneer results may be due to a mismodeling of the solar thermal contribution, but this significant discrepancy does raise questions.

Turyshev et al.'s results aside, the discrepancy between the theoretical value of $(1.5 \pm 0.4) \times 10^{-10}$ m s^{-2} and the absence of any such observed value, at least within the inner solar system (≤ 20 AU), needs to be addressed. In Penner [12] it was hypothesized that given that the solar magnetic field density increases rapidly as the Sun is approached, an electromagnetic field may in some manner inhibit the existence or lifetime of the proposed entities in the model. However, it is suspected that it is more likely that the semiclassical model of the behavior of the entities presented in Penner [12] is too simplistic and that the model as given breaks down in the stronger gravitational fields of the solar system. An improved model will have to wait though, for at the present time the focus of the author is to demonstrate that the theory of an induced energy polarized vacuum will explain observations that relate to the behavior of galaxies. In this regime the fields are weak enough so that the current modeled behavior of the entities is adequate.

References

1. Y. Sofue. Astrophys. J. **458**, 120 (1996). doi:10.1086/176796.
2. Y. Sofue, Y. Tutui, M. Honma, A. Tomita, T. Takamiya, J. Koda, and Y. Takeda Astrophys. J. **523**, 136 (1999). doi:10.1086/307731.
3. E. Noordermeer, J.M. van der Hulst, R. Sancisi, R.S. Swaters, and T.S. van Albada. Mon. Not. R. Astron. Soc. **376**, 1513 (2007). doi:10.1111/j.1365-2966.2007.11533.x.
4. R.B. Tully and J.R. Fisher. Astron. Astrophys. **54**, 661 (1977).
5. S.S. McGaugh, J.M. Schombert, G.D. Bothun, and W.J. DeBlok. Astrophys. J. **533**, L99 (2000). doi:10.1086/312628. PMID:10770699.
6. S.S. McGaugh and J. Wolf. Astrophys. J. **722**, 248 (2010). doi:10.1088/0004-637X/722/1/248.
7. M. Milgrom. New Astron. Rev. **46**, 741 (2002). doi:10.1016/S1387-6473(02)00243-9.
8. M. Milgrom. Astrophys. J. **270**, 365 (1983). doi:10.1086/161130.
9. M. Milgrom. Ann. Phys. **229**, 384 (1994). doi:10.1006/aphy.1994.1012.
10. P.D. Mannheim. Prog. Part. Nucl. Phys. **56**, 340 (2006). doi:10.1016/j.ppnp.2005.08.001.
11. A.R. Penner. Can. J. Phys. **89**, 841 (2011). doi:10.1139/p11-063.
12. A.R. Penner. Can. J. Phys. **90**, 315 (2012). doi:10.1139/p2012-029.
13. Y. Sofue. Publ. Astron. Soc. Jpn. **64**, (Manuscript in preparation) (2012).
14. Y. Sofue, M. Honma, and T. Omodaka. Publ. Astron. Soc. Jpn. **61**, 227 (2009).
15. Y. Sofue. Publ. Astron. Soc. Jpn. **61**, 153 (2009).
16. X.X. Xue, H.W. Rix, G. Zhao, et al. Astrophys. J. **684**, 1143 (2008). doi:10.1086/589500.
17. M. Honma, T. Bushimata, Y.K. Choi, et al. Publ. Astron. Soc. Jpn. **59**, 889 (2007).
18. C.S. Oh, H. Kobayashi, M. Honma, et al. Publ. Astron. Soc. Jpn. **62**, 101 (2010).
19. M.J. Reid, K.M. Menten, X.W. Zheng, et al. Astrophys. J. **700**, 137 (2009). doi:10.1088/0004-637X/700/1/137.
20. C. Flynn, J. Holmberg, L. Portinari, B. Fuchs, and H. Jahreib. Mon. Not. R. Astron. Soc. **372**, 1149 (2006). doi:10.1111/j.1365-2966.2006.10911.x.
21. J.D. Anderson, P.A. Laing, A.S. Lau, M.M. Nieto, and S.G. Turyshev. Phys. Rev. Lett. **81**, 2858 (1998). doi:10.1103/PhysRevLett.81.2858.
22. J.D. Anderson, P.A. Laing, A.S. Lau, M.M. Nieto, and S.G. Turyshev. Phys. Rev. D, **65**, 082004 (2002). doi:10.1103/PhysRevD.65.082004.
23. S.G. Turyshev and V.T. Toth. Living Rev. Relativ. **13**, 4 (2010). Available from: http://www.livingreviews.org/lrr-2010-4.
24. S.G. Turyshev, V.T. Toth, G. Kinsella, S. Lee, S. Lok, and J. Ellis. Phys. Rev. Lett. **108**, 241101 (2012). doi:10.1103/PhysRevLett.108.241101. PMID:23004253.